

Final Draft
of the original manuscript:

Ghobadi, E.; Heuchel, M.; Kratz, K.; Lendlein, A.:
**Influence of the addition of water to amorphous switching
domains on the simulated shape-memory properties
of poly(l-lactide)**
In: Polymer (2013) Elsevier

DOI: 10.1016/j.polymer.2013.05.064

Influence of the addition of water to amorphous switching domains on the simulated shape-memory properties of poly(*L*-lactide)

E. Ghobadi, M. Heuchel, K. Kratz, A. Lendlein*

Institute of Biomaterial Science, Helmholtz-Zentrum Geesthacht, Kantstr. 55, 14513 Teltow, Germany

*E-mail: andreas.lendlein@hzg.de

Phone: +49 (0) 3328 352 450

Fax: + 49 (0) 3328352 452

Abstract

It is well known that the environmental conditions e.g. humidity can alter the shape-memory properties of polymers. In this work we applied an atomistic molecular dynamics simulation approach to model the influence of the addition of 1 wt% and 2 wt% water on the simulated shape-memory behavior of the amorphous switching domains of poly(*L*-lactide) (PLLA) with a molecular weight of $M_n = 52,000 \text{ g}\cdot\text{mol}^{-1}$. For the dry as well as the water swollen PLLA-models, two subsequent uniaxial thermomechanical test cycles have been calculated, whereby the applied uniaxial deformation ε_m was varied between 50% and 150%.

All simulated PLLA models showed high shape fixity ratio of $R_f \geq 84\%$. The shape-memory properties obtained at $\varepsilon_m = 100\%$ for the dry PLLA and the models containing 1 wt% water were almost identical with a shape recovery ratio in the first and second test cycle around $R_r = 61\% - 64\%$. In contrast PLLA with 2 wt% water exhibited higher values of $R_r = 76\%$ during the first test cycle, but a lower $R_r = 52\%$ in the subsequent second cycle. Furthermore, increasing the applied ε_m resulted in a decrease of R_r from 82% to 42% for the dry PLLA, whereas PLLA with 2 wt% water did not show a dependence of R_r on ε_m . We anticipate that these observations can be attributed to differences in the initial structure of the various simulated PLLA models e.g. the different distribution of the free volume elements.

1. Introduction

The observation that the shape-memory capability of certain thermo-sensitive polymers can be significantly influenced or even triggered by the uptake of water has attracted high scientific and technological interest and is of great relevance for manifold applications such as medical devices or textiles [1-5]. A thermally-induced shape-memory effect (SME) of a polymer is its ability to maintain a deformed temporary shape that is established after application of a specific thermomechanical treatment called shape-memory creation procedure (SMCP). Such a programmed shape-memory polymer (SMP) can shift back to the memorized original shape (before deformation) when a certain switching temperature T_{sw} is exceeded [6, 7]. The recovery force is driven by the entropy gained by the switching chain segments, when moving from an oriented (programmed) conformation to a random coil-like (recovered) chain conformation. The characteristic T_{sw} , which can be determined as inflection point of the strain-temperature recovery curve under stress free conditions [8] is related to the thermal transition (T_{trans}) of the switching domains acting as reversible crosslinks. T_{trans} can be a glass transition (T_g) or a melting temperature (T_m). A typical “heating-deformation-cooling” SMCP consists of deforming the polymer at temperatures above T_{trans} , followed by cooling to temperatures below T_{trans} while keeping the external load, whereby the reversible crosslinks solidify and finally the external stress is removed (unloading) to obtain the fixed temporary shape.

In recent studies it was shown that the environmental conditions such as the humidity can substantially influence the shape-memory properties of polymers [9-12]. These findings motivated the development of the concept of a moisture triggered SME [13-16]. The underlying mechanism is either the water induced dissolution of crystalline domains, as observed for copolymer networks containing grafted crystallizable PEG side chains [17] or the disintegration of hydrogen bonds in polyurethanes [13], a substantial decrease in T_g accompanied by softening of the polymer matrix as a result of the water uptake, which is reported in particular in SMPs with amorphous switching domains [14].

The shape-memory properties of polymers have been mainly studied experimentally e.g. by conducting cyclic thermomechanical tests [18-22]. Important characteristics for quantification of the shape-memory properties are the shape fixity ratio (R_f), which describes the capability of a polymer to temporarily fix an applied deformation ϵ_m and the shape recovery ratio (R_r) characterizing how well the original permanent shape is recovered. Furthermore, diverse theoretically modeling approaches have been reported to simulate or investigate the SME of

polymers, including different constitutive models [23-28], but also molecular simulation methods [29-33]. In this context we recently introduced a molecular dynamic modeling approach, which could successfully describe two subsequent thermomechanical cycles of amorphous PLLA switching segments [34, 35]. As in our former studies, we assume that the crystalline domains in the semicrystalline thermoplastic PLLA represent the physical netpoints that only transfer stress to the viscoelastic amorphous domains and provide the permanent shape. The amorphous domains are the switching segments responsible for fixing the temporary shape, and recoiling of the chain segments above T_{sw} .

The aim of this study was to explore whether the incorporation of water molecules into an amorphous PLLA matrix can influence the simulated shape-memory properties. Dry PLLA models as well as moist models containing 1 wt% and 2 wt% water content were constructed and their free volume elements distributions as well as the related changes in T_g were examined. The lower value is in the range of the estimated experimental equilibrium water uptake at room temperature. Based on the extrapolation of experimental water sorption data at 308 K [36] to a water activity of 1.0, and assuming that sorption takes place only in the amorphous domains, a maximum value of 1.3 wt%-1.4 wt% can be expected in accordance to experimental results for a completely amorphous sample [37]. For quantification of the shape-memory properties, a simulated cyclic thermomechanical test consisting of two subsequent cycles with uniaxial deformations of 100% was applied for the dry and the two moist packing models. Additionally, the same procedure consisting of two subsequent test cycles was carried out with $\epsilon_m = 50\%$ and 150% for the dry and the 2 wt% water swollen system. Following the previous studies with PLLA [34, 35], as reference temperatures $T_{low} = 250$ K and $T_{high} = 500$ K were selected, as preliminary studies conducted at $T_{high} = 450$ K did not result in any shape recovery over a simulation time up to some nanoseconds. Finally, the relaxation kinetics during unloading at $T_{low} = 250$ K and the recovery kinetics at $T_{high} = 500$ K were analyzed by application of a Voigt model approach.

2. Simulation experiments

Molecular dynamics (MD) simulations were carried out with the Material Studio (MS 5.0) and Discover software packages by Accelrys. All simulations were run on 4- to 16-CPU nodes of a 92 CPU RedHat Linux cluster. The calculations were performed with the COMPASS forcefield which is a density optimized forcefield that can predict density values

with an accuracy comparable with experiments [38]. The nonbond interactions were treated with a group based summation method using a cutoff of 12.5 Å.

2.1. Preparation of atomistic packing models for dry and water swollen amorphous PLLA

Three independent amorphous packing models (a, b, c) were constructed for each of three systems: PLAw0 consists of a single PLLA chain with 720 repeating units and a molecular weight of $M_n = 52,000 \text{ g}\cdot\text{mol}^{-1}$. The systems PLAw1 and PLAw2 were also composed from a PLLA chain of the same length but with additionally 1 wt% and 2 wt% water, respectively.

At $T = 500 \text{ K}$, i.e. in the completely molten state of PLLA, following the Theodorou-Suter method [39] and using an initial target density of $\rho = 1.0 \text{ g}\cdot\text{mol}^{-1}$, packing models were constructed. The so constructed models were afterwards equilibrated according to the stepwise methodology described in Ref. [40], which includes repeated energy minimizations and MD-steps connected with a scaling of forcefield parameters for torsion and nonbond interaction terms. Afterwards an annealing procedure was carried out consisting of short 50 ps *NVT*-MD simulation steps for decreasing temperatures from $T = 900 \text{ K}$ to 500 K. As final step, for data production stage, and to ensure that the simulating model systems are reliable, a 2.5 ns *NPT*-MD simulation at $T = 500 \text{ K}$ and at a constant ambient pressure of $P = 0.1 \text{ MPa}$ was carried out. Temperature and pressure were controlled in the MD simulations with the Berendsen thermostat [41] and Andersen barostat [42]. All MD simulations showed stable volume fluctuations at the final temperature of 500 K. The packing models at this stage have a cubic structure.

2.2 Volumetric swelling and partial molar volume

The volume of a polymer system may change when small penetrants enter the matrix. This change is known as a volumetric swelling (or volumetric dilation). If V_{dry} is the volume of the model in dry state and V_{wet} is the volume of water swollen model (after incorporation of water), the volumetric dilation D (swelling) is then defined as the volume change ΔV relative to the volume of the initial dry state V_{dry} and can be calculated from Eq. (1):

$$D = \frac{\Delta V}{V_{\text{dry}}} = \frac{V_{\text{wet}} - V_{\text{dry}}}{V_{\text{dry}}} \times 100\% \quad (1)$$

The Volumetric dilation effect can also be related to the partial molar volume \bar{V}_p of water. The \bar{V}_p values can be estimated as the ratio of volume change ΔV to the change in water concentration Δc that has caused the volume change $\bar{V}_p = \Delta V / \Delta c$. It should be noted, that in

case the small penetrant molecules would only occupy parts of the existing free volume between the polymer chains, ΔV may be zero, and consequently also D and \bar{V}_p .

2.3 Characterization of free volume

The fractional free volume (FFV) of polymers is usually related to the transport of small penetrants into a polymeric system and also to the configuration and interaction of the polymer chains to each other and to other small molecules in the system. Not only the total amount of free volume but also the particular distribution of fractional free volume elements is expected to influence considerably the material properties.

The FFV accessible for water molecules in the dry and swollen packing models was determined according to Ref. [43]. All atoms of the polymer were represented through hard spheres of respective radius. Then a three dimensional grid was superimposed over the cubic boxes of the polymer packing models. Afterwards, at every point of this grid, a hard sphere (test particle) with a radius of 1.5 Å (equivalent to the radius of a water molecule [44]) was placed and it was checked whether the test particle and any atom of the polymer matrix overlap each other. If so, then the volume element around the respective grid point belongs to the occupied volume of the polymer chain and in the opposite case the volume element around the grid point belongs to the accessible free volume of the test particle in the packing model of the polymer. Finally all connected free volume elements were integrated.

2.4 Mobility of polymeric chains and water molecules

The mean square displacement of atoms of a polymer chain from their original location at a certain instant of time is related to the self-diffusion coefficient [45]. The self-diffusion of polymer chains in both dry and water swollen samples can be evaluated in terms of the mean square displacement (MSD) of the backbone atoms which can be calculated from Eq. (2):

$$MSD = \langle \Delta r^2(t) \rangle = \frac{1}{N} \sum_{i=1}^N (\vec{r}_i(t) - \vec{r}_i(t=0))^2 \quad (2)$$

where $\vec{r}_i(t)$ is the coordinate vector of atom i at time t and $\vec{r}_i(t=0)$ is the respective location of this atom at the initial point of time.

2.5 Simulation of uniaxial stretching

Equilibrated packing models were uniaxially stretched with *NPT*-MD simulation using the Parrinello-Rahman barostat [46]. With the Parrinello-Rahman (PARA) barostat, external

stress tensor values can be specified so that the stretching of the samples in a certain direction will be allowed. The size change of the simulation box into every spatial direction during stretching simulations is observed by the temporal extension values $\varepsilon(t)$

$$\varepsilon_i(t) = (L_i(t) - L_{0i}) / L_{0i} \quad (3)$$

where $i = x, y, z$ represents the three spatial directions. $L_i(t)$ and $L_{0i} = L_i(t = 0)$ are the box length in i -direction at simulation time t , and the respective initial value at the beginning of the stretching calculations.

Under periodic boundary conditions with the minimum image convention, stretching simulations were carried out to obtain fixed maximum extension values in uniaxial (x -) direction of $\varepsilon_m = 50\%$, 100% and 150% . At $T = 500$ K, applying the Berendsen thermostat with a decay constant of 0.1, a constant symmetrical stress matrix was chosen with non-diagonal terms equal to zero and the initial diagonal components as: $\sigma_{ii} = \{50, -0.1, -0.1\}$ MPa. This pressure tensor was applied for the first 1.0 ns with a time step of $\Delta t = 0.5$ fs. If the finally obtained extension value $\varepsilon(t = 1\text{ns})$ was considerably below the target extension ε_m , the applied stress tensor value in x -direction was increased to $\sigma_{xx} = 80$ MPa in the next ns. The dimensionless cell mass parameter in the PARA barostat was always $w = 20$.

2.6 Simulation steps of a uniaxial thermomechanical cycle

The uniaxial thermomechanical test cycles modeled here, consist of a strain-controlled programming and stress-free recovery procedure. They are realized in four steps: (i) stretching the model at T_{high} ($T_{\text{high}} > T_{\text{sw}}$) to a certain extension ε_m , (ii) cooling to T_{low} ($T_{\text{low}} < T_{\text{sw}}$), (iii) unloading at T_{low} , and finally (iv) reheating from T_{low} to T_{high} under stress free condition to recover the permanent shape, characterized by the recovered extension ε_p . This cycle can be repeated to simulate multiple subsequent test cycles, where the parameters T_{low} , T_{high} , and ε_m are kept constant.

Step (i) was realized at $T_{\text{high}} = 500$ K with the uniaxial stretching simulations described in section 2.5. The obtained shape is called the stretched shape.

The cooling to T_{low} in step (ii) was modeled with a *NVT*-MD simulation of 1.0 ns at $T_{\text{low}} = 250$ K, in which the Berendsen thermostat with a decay constant of 0.1 and a time step of $\Delta t = 0.5$ fs was used.

Step (iii), the unloading to zero stress ($\sigma = 0$) at T_{low} , was modeled by a *NPT*-MD simulation of $t = 1.0$ ns applying the PARA barostat. The stress-free condition is realized with the tensor

values $\sigma_{ii} = \{-0.1, -0.1, -0.1\}$ MPa, corresponding to hydrostatic ambient pressure condition. Result is the temporary fixed shape characterized by an extension value ε_u , also called the programmed shape.

The last step (iv) of the cycle was simulated as T -jump from T_{low} to $T_{\text{high}} = 500$ K followed by a long NPT -MD simulation (up to $t = 6.0$ ns) again with the PARA barostat and hydrostatic pressure condition. The recovered shape after completion of the shape-memory cycle is characterized by the permanent extension ε_p .

2.7 Quantification of the shape-memory effect

In cyclic thermomechanical tensile tests, the shape-memory capability of a SMP is typically characterized by the shape fixity ratio (R_f) and the shape recovery ratio (R_r). R_f characterizes the ability of a system to fix its temporary shape and R_r is the recoverability of the permanent shape. R_f and R_r values can be calculated according to the following equations (4) and (5) respectively:

$$R_f = \frac{\varepsilon_u(N)}{\varepsilon_m} \times 100\% \quad (4)$$

$$R_r = \frac{\varepsilon_m - \varepsilon_p(N)}{\varepsilon_m - \varepsilon_p(N-1)} \times 100\% \quad (5)$$

where ε_m is the applied maximum extension, $\varepsilon_u(N)$ is the strain achieved after completion of the programming in the N th cycle and $\varepsilon_p(N)$ is the residual strain after recovery at T_{high} in the N th cycle.

3. Results and discussion

3.1 Influence of water uptake on density, free volume and T_g of PLLA

The influence of the addition of water molecules on the material properties such as density or free volume was investigated with unstretched PLLA packing models.

The equilibrated samples at $T_{\text{high}} = 500$ K were prepared according to the procedure presented in section 2.1 and are the basis for the MD simulations of the shape-memory cycles. It should be emphasized that our models present exclusively the amorphous parts of PLLA and not crystalline parts of this semicrystalline material (for more details see Ref. [34]). After the final equilibration simulation at T_{high} , densities of the unstretched ($\varepsilon_m = 0\%$) samples were

calculated. Here an averaged density of $\rho = 1.057 \text{ g}\cdot\text{cm}^{-3}$ for the PLAw0 was obtained, which is in good agreement with the experimental density of $1.07 \text{ g}\cdot\text{cm}^{-3}$ for a PLLA melt with $M_n = 50,000 \text{ g}\cdot\text{mol}^{-1}$ at 500 K [47]. Packing models with 1 wt% water contained additionally 30 water molecules and reached an average density of $1.051 \text{ g}\cdot\text{cm}^{-3}$ at T_{high} . This value decreases to $1.035 \text{ g}\cdot\text{cm}^{-3}$ for samples with 2 wt% H₂O content (equivalent to 60 water molecules). Structural characteristics of the unstretched equilibrated dry and water swollen samples are listed in supplementary Table S1 (see Appendix).

The partial molar volume and the volumetric swelling of the samples have been calculated from the average volume of the samples during the final *NPT* MD-simulations according to the method previously described in Ref. [48]. The averaged swelling effect of water on the unstretched packing models at $T_{\text{high}} = 500 \text{ K}$ was about $D = 2.0 \pm 0.4\%$ and $D = 4.0 \pm 0.1\%$ for a water content of 1 wt% and 2 wt% respectively. This effect is related to partial molar volumes of water of $\bar{V}_p = 31 \pm 6 \text{ cm}^3\cdot\text{mol}^{-1}$ (PLAw1) and $41 \pm 4 \text{ cm}^3\cdot\text{mol}^{-1}$ (PLAw2). These values are higher than the \bar{V}_p value of liquid water at room temperature ($\bar{V}_p = 18 \text{ cm}^3\cdot\text{mol}^{-1}$). The high \bar{V}_p values indicate the condition of water in a vapor state. We have also calculated the swelling effect at $T = 300 \text{ K}$ (room temperature) for 2 wt% water content and obtained a value of $D = 2.1\%$ with the respective partial molar volume of $15.6 \text{ cm}^3\cdot\text{mol}^{-1}$. This value is lower than for pure water. In a recent simulation study about swelling effects of poly(lactide-*co*-glycolide) (PLGA), comparable values have been reported [49]. It seems that at room temperature water molecules (up to 2 wt% water) fill the existing free volume elements of PLLA and PLGA. In another work, for samples of PLLA with 19 chains and 50 repeating units a smaller volumetric swelling ($D = 1.02\%$) was calculated at $T = 310 \text{ K}$ [48].

For determination of free volume elements in the water swollen packing models (PLAw1 and PLAw2), the water molecules were removed. Fig. 1a presents the distribution of free volume elements of the dry (PLAw0) and the swollen PLLA matrices. The free volume elements are presented by the radius of a sphere of equivalent volume. The integral area over the columns is a measure for the total fractional free volume of the polymer matrix.

As expected the dry PLAw0 samples showed the smallest fractional free volume accessible for water. The radius of FFV elements is in the range of about 1 - 5 Å. The FFV increases with the increase of the amount of water incorporated in the polymer matrix. The largest FFV belongs to the PLAw2 samples. The mean radius of the cavities changes only insignificantly by increasing the amount of water (2.16 Å for PLAw0, 2.26 Å for PLAw1, and 2.43 Å for

PLAw2). However PLAw2 showed also cavities with radii larger than 5.0 Å. These results are similar to previously reported data of simulated PLGA models presented in Ref. [49].

The averaged MSD curves for backbone atoms in the dry and the water swollen states at $T_{\text{high}} = 500$ K are displayed in Fig. 1b. The mobility of backbone atoms at T_{high} is significantly higher than at room temperature where after one nanosecond a MSD of about 3 \AA^2 is reached (not presented here). At $T_{\text{high}} = 500$ K a much higher mobility of the backbone atoms is observed. Fig. 1b shows a certain influence of water content on the mobility of polymer atoms. For dry models (PLAw0) and water swollen models with 1 wt% water content (PLAw1) similar MSD values were obtained, whereby PLAw1 exhibited slightly higher values. In contrast for PLAw2 containing 2 wt% of water, the backbone atoms had significantly higher mobilities (see open red triangles in Fig. 1b). The increase in mobility of backbone atoms with higher water content in the polymer matrix can be understood as a consequence of the water induced swelling effect which resulted in an increased space between chain segments. The behavior of the model system corresponds to the experimentally observed plasticizing effect [50].

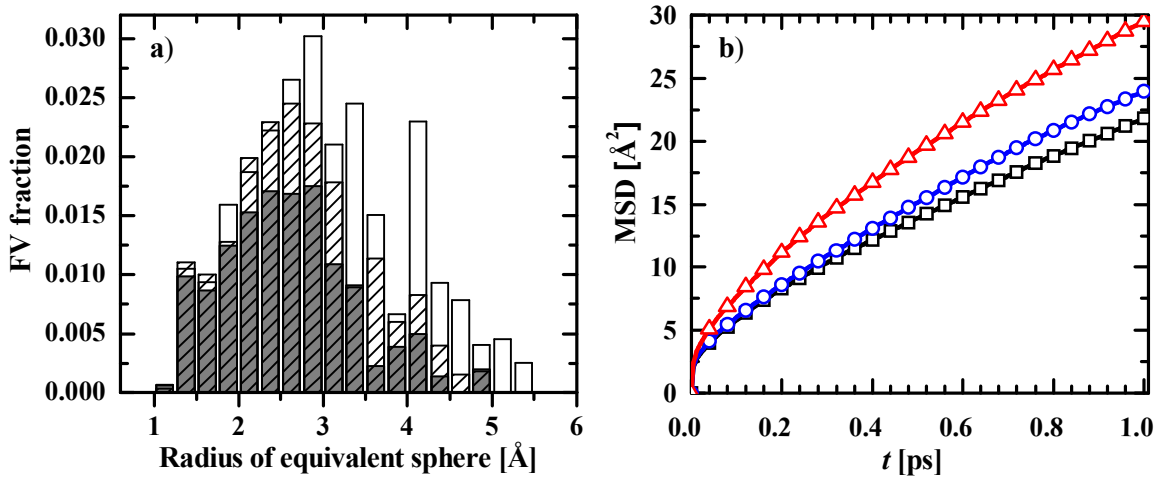


Fig. 1. a) Distribution of free volume elements accessible for water at $T = 500$ K in PLLA matrices in the dry state (PLAw0, gray fasciated) and after swelling with 1 wt% water (PLAw1, white fasciated) and 2 wt% water (PLAw2, white). b) Mean square displacement (MSD) of backbone atoms vs. time for dry and water swollen PLLA samples at $T_{\text{high}} = 500$ K (<PLAw0>: open black squares, <PLAw1>: open blue circles and <PLAw2>: open red triangles).

To survey the influence of water molecules on the volumetric properties and consequently on the glass transition temperature T_g of amorphous PLLA packing models, specific volume V_{sp} data of simulated PLAw0, PLAw1 and PLAw2 models are depicted in Fig. 2. The presented V_{sp} data were obtained via NPT MD-simulations according to the method recently described in Ref. [34].

For the dry PLLA system (PLAw0, open squares) a good agreement with the experimental specific volume data was observed at temperatures > 450 K, where PLLA is completely molten. Almost similar results have been reported for systems with shorter PLLA chains [34].

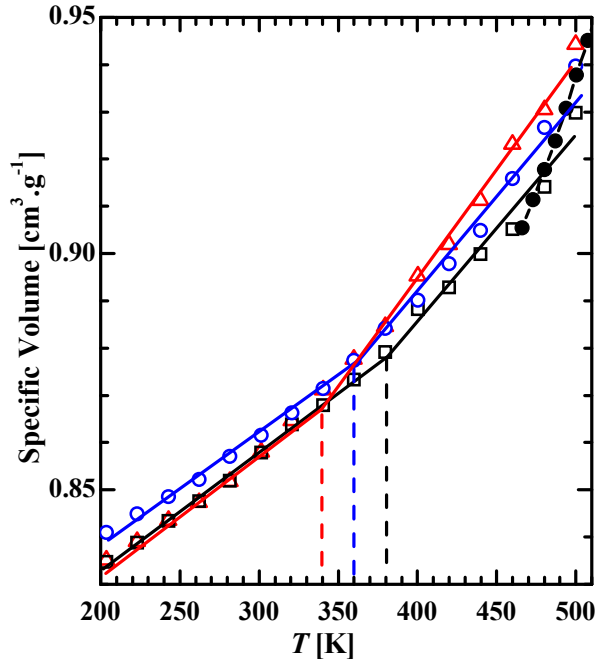


Fig. 2. Simulated mean specific volume V_{sp} vs. temperature T for dry (PLAw0: open black squares) and water swollen amorphous PLLA packing models (PLAw1 with 1 wt% water content: open blue circles; and PLAw2 with 2 wt% water content: open red triangles) calculated with NPT -MD at $P = 0.1$ MPa during cooling from 500 K to 250 K in comparison with experimental data of a semicrystalline ($w_c = 0.37$) PLLA sample [47]. Vertical dotted lines mark the simulated glass transition temperatures.

The simulated data in Fig. 2 for dry and water swollen models show that the specific volume diminishes with decreasing temperature from T_{high} . Below T_g , the decrease of specific volume with decreasing temperature is less pronounced and produces a kink in the $V_{sp} - T$ curve. One can distinguish nearly two linear ranges, the melt range at higher temperatures with a larger slope (representing the thermal expansion coefficient) and at lower temperatures the glassy range with a lower slope. A first approximate estimation of the kink point has been yielded by visual inspection of data points. They are divided into two groups corresponding to those below and above glass transition temperature. Afterwards each of these groups has been fitted by linear fit-lines, resulting in two different gradients. The cross-section of these two fit-lines estimates the simulation glass transition temperature [51]. The vertical dotted lines in Fig. 2 point where the simulated glass transition temperature of the model systems is located.

For dry <PLAw0> packing models, a glass transition value of about $T_g \approx 380$ K was found. Experimental T_g values for PLLA are in the range of 330 to 340 K which are obtained by differential scanning calorimetry at heating rates of $10 \text{ K} \cdot \text{min}^{-1}$ [52]. In our previous work for dry PLLA models with shorter chains, a slightly higher T_g could be calculated, if the points in

the $V_{sp} - T$ curves were fitted with the same procedure explained above [34]. The difference between the simulated and experimental T_g might be attributed to the extreme cooling rate in the order of $10^{11} \text{ K}\cdot\text{s}^{-1}$ during the simulation compared to typical experimentally applied cooling rates around $10 \text{ K}\cdot\text{min}^{-1}$.

Moreover it is well known [53] that water can have a plasticization/softening effect on polymer materials resulting in a shift of T_g to lower temperatures. From the simulated V_{sp} -curves of the dry PLLA system (PLAw0) in comparison to the two water swollen samples displayed in Fig. 2 such a shift of T_g towards lower T -values with $T_g \approx 360 \text{ K}$ (PLAw1) and $T_g \approx 340 \text{ K}$ (PLAw2) becomes obvious. Experimentally, a clear plasticization effect of small amounts of water in PLLA was determined by dielectric spectroscopy [54].

3.2 Influence of water on a thermomechanical test cycle of PLLA

The equilibrated dry and water swollen packing models were stretched according to the PARA approach at $T_{\text{high}} = 500 \text{ K}$ (see section 2.6). Results for stretching of the samples to $\epsilon_m = 100\%$ in x -direction as a function of time under applied stress regime of $\sigma_{xx} = 50 \text{ MPa}$ for the first nanosecond ($0 \text{ ns} < t \leq 1.0 \text{ ns}$) and afterwards ($1.0 \text{ ns} < t$) at $\sigma_{xx} = 80 \text{ MPa}$ are presented in Fig. 3a.

The packing models of PLAw0 and PLAw1 show initially more resistance to the applied stress and therefore the increase of the extension per time unit is lower. The obtained mean extension values of these samples overlap each other, so that for both dry and water swollen samples (with 1 wt% water) a qualitative similar behavior in the uniaxial stretching at T_{high} step (i) can be observed. Here slightly different apparent extension values of about 35% (PLAw0) and 50% (PLAw1) were obtained at the end of the first stretching period after 1 ns ($\sigma_{xx} = 50 \text{ MPa}$). In contrast a characteristically different stretching behavior was observed for PLAw2, whereby an apparent extension value of about 85% was reached after 1 ns at $\sigma_{xx} = 50 \text{ MPa}$. The different response of dry and wet samples to an external force can be related to the plasticization/softening effect caused by the incorporated water molecules.

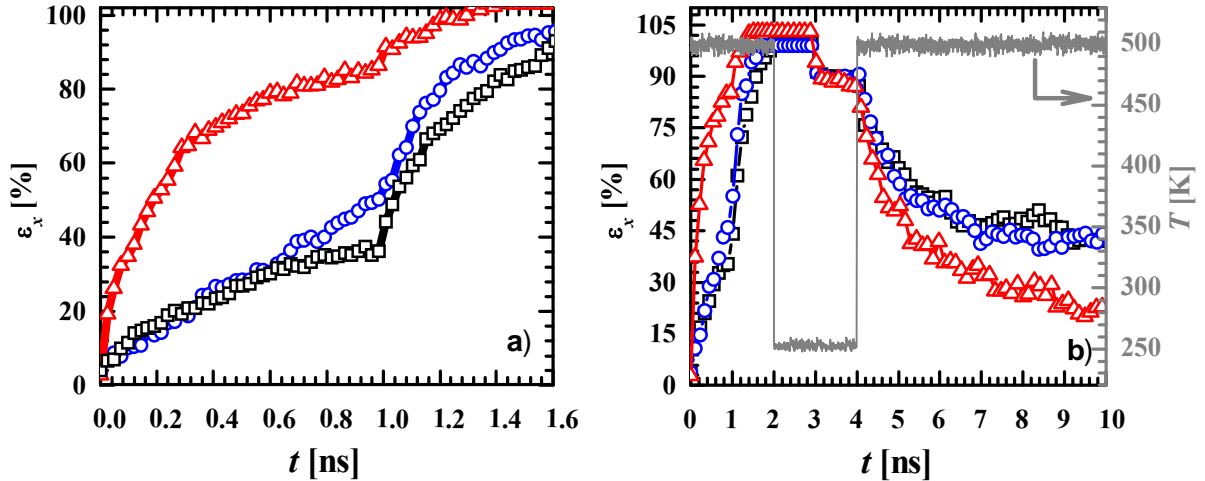


Fig. 3. a) Evaluation of uniaxial deformation of PLLA samples under PARA conditions with different water content: <PLAw0>: open black squares, <PLAw1>: open blue circles, <PLAw2>: open red triangles.

b) Simulated shape-memory cycle of dry and water swollen samples, the corresponding T -values are plotted as gray line with respect to the right ordinate. <PLAw0>: open black squares, <PLAw1>: open blue circles, <PLAw2>: open red triangles

In order to study the influence of moisture on the macroscopic behavior of water swollen packing models, every system was subjected to a complete simulated thermomechanical cycle as described in Section 2.6. Models were uniaxial stretched in step (i) under the same stress tensor till they reached extension values corresponding to $\varepsilon_m = 50\%$, 100% , and 150% with correspondingly longer simulation time. From this point on, the next steps of the shape-memory simulation (unloading at T_{low} and recovery at T_{high}) followed the same time sequence. All samples showed a fast relaxation within the first 50 ps after unloading (step iii) and reached a ε_u value of about 90%, which is equivalent to a shape fixity ratio of $R_f = 90\%$ (see Fig. 3b). The observed relaxation process can be related to energy stored in the stretched PLLA models. Finally, starting from the temporary fixed shape ε_u at $t = 4.0$ ns the recovery simulations were performed by a T -jump from T_{low} to T_{high} , followed by NPT MD-simulation for at least 6 ns under ambient pressure conditions with the PARA barostat. Both, dry models and water swollen packing models exhibited a similar shape recovery behavior, whereby PLAw2 showed a higher initial recovery rate and reached higher shape recovery values of $R_r = 76\%$ (see Fig. 3b and Table 1). We attributed this observation to the higher mobility of polymeric chains in water swollen states, which may be related to the increase of free volumes between polymeric chains.

3.3 Influence of maximum extension ε_m on shape-memory properties

In order to study the influence of the applied ε_m on the shape-memory properties of PLLA PLAw0 and PLAw2 packing models were additionally investigated by thermomechanical tests with $\varepsilon_m = 50\%$ and 150% . In the following, at first the influence of ε_m on the unloading step (iii) and R_f will be discussed and afterwards the impact on the shape recovery behavior and R_r .

The relative extension values $\varepsilon_x/\varepsilon_m$ presented in Fig. 4 can be understood as the temporal development of the apparent shape fixity ratio $R_{f,app}$ during unloading at $T_{low} = 250$ K. After a time period of approx. 200 ps the decay in $\varepsilon_x/\varepsilon_m$ is almost completed and a plateau value in the range of $R_{f,app} = 84\%-93\%$ was reached in all experiments. For the dry model system PLAw0 raising ε_m from 50% to 150% resulted in an increase of $R_{f,app}$ from 86% to 93% (Fig. 4a and Table 1). In contrast the unloading process as well as R_f of PLAw2 systems was not affected by the variation of ε_m (Fig. 4b and Table 1).

Table 1 Summary of calculated strain fixity ratio R_f and strain recovery ratio R_r of PLLA packing models with different water content after 1st and 2nd simulated shape-memory cycles stretched up to different maximum strains ε_m

Model ID ^{a)}	ε_m ^{b)} [%]	$R_f(1)$ ^{c)} [%]	$R_r(1)$ ^{c)} [%]	$R_f(2)$ ^{c)} [%]	$R_r(2)$ ^{c)} [%]
<PLAw0>	50	84 ± 4	81 ± 8	-	-
<PLAw0>	100	89 ± 2	62 ± 3	89 ± 2	62 ± 1
<PLAw0>	150	93 ± 2	42 ± 5	-	-
<PLAw1>	50	-	-	-	-
<PLAw1>	100	92 ± 2	64 ± 4	89 ± 1	61 ± 1
<PLAw1>	150	-	-	-	-
<PLAw2>	50	88 ± 4	61 ± 5	-	-
<PLAw2>	100	88 ± 3	76 ± 2	93 ± 2	52 ± 2
<PLAw2>	150	89 ± 5	66 ± 4	-	-

^{a)}<PLAw0>, <PLAw1>, <PLAw2> represent <averages> of three PLLA models consisting each of a single chain and 0 wt%, 1 wt%, and 2 wt% water content, respectively.

^{b)} Maximum stretching length

^{c)} Obtained average and standard deviation out of three individual packing models

For a further quantification of the relaxation process related to the unloading step (iii), the data points were fitted with the following single exponential decay function:

$$r_\varepsilon = \frac{\varepsilon_x(t)}{\varepsilon_{ref}} = r_\varepsilon^\infty + E^* \exp\left(-\frac{t}{\tau}\right) \quad (6)$$

where the reference extension ε_{ref} is ε_m in case of the unloading step or ε_u for the recovery step (iv) which will be discussed later. The changes in length of the samples during unloading process are considered as creep relaxation to non-recoverable residue described by Voigt model. Here E^* and τ present the elastic module of a spring and relaxation time of a dashpot respectively, while r_{ε^∞} is the infinite $\varepsilon_x/\varepsilon_m$ value after infinite time, which is equivalent to R_f . The solid lines in Fig. 4 are the obtained fitting curves and the calculated E^* , τ and r_{ε^∞} as well as the factor $-E/\tau$ as a measure for the initial recovery speed are listed in the upper half of Table 2. This analysis revealed that for the dry PLLA model systems E^* decreased from 0.138 to 0.069 with increasing ε_m , while short relaxation times with $\tau \leq 0.01$ ns were obtained for the relaxation kinetics. In contrast the PLAw2 models exhibited almost constant values for E^* around 0.110 and the τ values were found to increase from 0.01 ns ($\varepsilon_m = 50\%$) to 0.06 ns at $\varepsilon_m = 150\%$, whereby the initial recovery speed $-E/\tau$ was significantly lower compared to PLAw0. We attributed these findings to the higher density and the lower mobility of PLLA chains in the dry state, which allows a better fixation for higher applied deformations, because of the higher interaction between the oriented single PLLA chains.

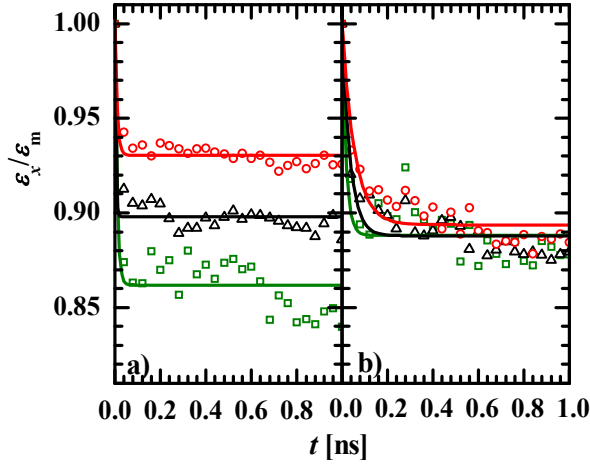


Fig. 4. Temporal development of averaged extension values in relative units ($\varepsilon_x/\varepsilon_m$) for the “unloading” step at $T_{low} = 250$ K for different applied ε_m values ($\varepsilon_m = 50\%$: open green squares, $\varepsilon_m = 100\%$: open black triangles, $\varepsilon_m = 150\%$: open red circles) in the programming step. PLAw0 (left panel) and PLAw2 (right panel).

Table2. Results obtained by analysis of the simulated unloading (Unl.) and recovery (Rec.) processes according to the model description of eq. (6) for PLAw0, PLAw1 and PLAw2 samples at different ε_m and two subsequent test cycles (1st and 2nd).

Model ID ^{a)}	ε_m	Process	T [K]	$r_\varepsilon^{\infty b)}$	$E^* b)$	τ [ns]	$R^{2c)}$	$-E/\tau^d)$ [ns ⁻¹]
<PLAw0>	50%	1 st Cyc._Unl.	250	0.862	0.138	0.010	0.366	-14.5
<PLAw0>	100%	1 st Cyc._Unl.	250	0.898	0.102	0.003	0.543	-30.9
<PLAw0>	150%	1 st Cyc._Unl.	250	0.938	0.069	0.009	0.460	-7.5
<PLAw0>	100%	2 nd Cyc._Unl.	250	0.852	0.1472	0.035	0.539	-4.2
<PLAw1>	100%	1 st Cyc._Unl.	250	0.953	0.047	0.010	0.483	-1.1
<PLAw1>	100%	2 nd Cyc._Unl.	250	0.860	0.140	0.048	0.621	-2.9
<PLAw2>	50%	1 st Cyc._Unl.	250	0.888	0.112	0.018	0.402	-6.4
<PLAw2>	100%	1 st Cyc._Unl.	250	0.888	0.112	0.035	0.563	-3.2
<PLAw2>	150%	1 st Cyc._Unl.	250	0.893	0.106	0.055	0.553	-1.9
<PLAw2>	100%	2 nd Cyc._Unl.	250	0.905	0.094	0.021	0.561	-4.6
<PLAw0>	50%	1 st Cyc._ Rec.	500	0.340	0.660	0.894	0.895	-0.7
<PLAw0>	100%	1 st Cyc._ Rec.	500	0.481	0.519	1.197	0.926	-0.4
<PLAw0>	150%	1 st Cyc._ Rec.	500	0.618	0.382	0.501	0.808	-0.7
<PLAw0>	100%	2 nd Cyc._ Rec.	500	0.509	0.491	1.037	0.927	-0.5
<PLAw1>	100%	1 st Cyc._ Rec.	500	0.446	0.554	0.879	0.971	-0.6
<PLAw1>	100%	2 nd Cyc._ Rec.	500	0.466	0.534	2.113	0.806	-0.3
<PLAw2>	50%	1 st Cyc._ Rec.	500	0.488	0.512	0.748	0.903	-0.7
<PLAw2>	100%	1 st Cyc._ Rec.	500	0.288	0.712	1.066	0.956	-0.3
<PLAw2>	150%	1 st Cyc._ Rec.	500	0.420	0.580	1.031	0.929	-0.4
<PLAw2>	100%	2 nd Cyc._ Rec.	500	0.557	0.443	1.214	0.919	-0.4

^{a)}<PLAw0>, <PLAw1>, <PLAw2> represent <averages> of three PLLA models consisting each of a single chain and 0 wt%, 1 wt%, and 2 wt% water content, respectively.

^{b)}Standard deviation \pm 0.001.

^{c)}Correlation coefficient.

^{d)}Measure for the initial speed of the recovery process $d\varepsilon/dt$.

The different applied ε_m values influenced also the shape recovery process of the samples at T_{high} . Fig. 5 shows the temporal development of the strain of the samples stretched with different stretching lengths during the recovery step plus fit curves which will be discussed later.

Both dry (PLAw0) and water swollen (PLAw2) models showed a similar recovery behavior, whereby a plateau value for ε_p was reached within 6 ns simulation time. The obtained recovery processes at $T_{\text{high}} = 500$ K with τ values in the range of 0.5 to 2.1 ns were found to be more than one order of magnitude slower than the very fast relaxation of elastic stresses during unloading at $T_{\text{low}} = 250$ K. It should be noted that with a correlation coefficients R^2 between 0.80-0.97 (see Table 2), the recovery process is much better represented by the exponential decay function (6) as the unloading process, where this coefficient has only values between 0.37 and 0.62.

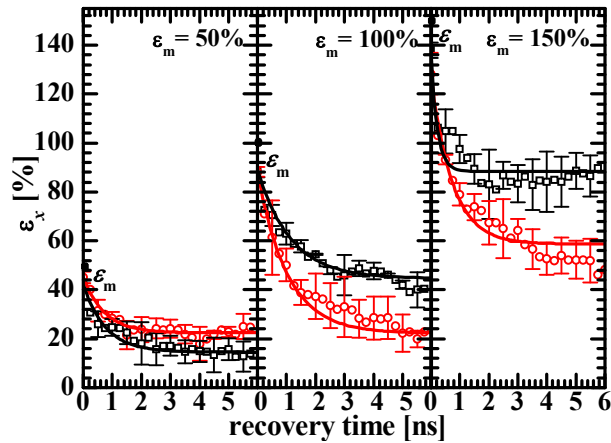


Fig. 5. Temporal development of extension values ε_x for the “recovery” step of PLAw0 (open black squares) and PLAw2 (open red circle) samples at $T_{\text{high}} = 500$ K for different ε_m of 50%, 100% and 150%.

The obtained fit parameters for the recovery step, presented in the lower half of Table 2 were similar to previously reported data with $\tau = 1.26$ ns for PLLA models with lower M_n of 13,000 $\text{g}\cdot\text{mol}^{-1}$ [34]. The initial recovery kinetics ($-E/\tau$) observed for the water swollen systems in the current study was not significantly faster compared to the dry PLLA (Table 2).

For all samples the magnitude of the achieved ε_p is higher as higher the applied ε_m was. While in the dry systems R_r was found to decrease from 82% to 42% when ε_m was increased, for PLAw2 shape recovery ratios in the range of 76%-61% were obtained (see Table 1). While at $\varepsilon_m = 50\%$ the PLAw0 system exhibited the higher R_r value, at higher extensions values of $\varepsilon_m = 100\%$ and $\varepsilon_m = 150\%$, the water swollen PLLA system showed a significantly higher shape recovery ratio.

In summary both the increase in R_r as well as the decrease in R_f with increasing ε_m in dry and water swollen PLLA samples can be explained by a higher degree of orientation of polymer chains and in this way a lower entropy of the systems at higher deformations.

3.4 Influence of water on two successive thermomechanical test cycles

Finally, we have investigated the shape-memory characteristics of dry and water containing models in two subsequent thermomechanical cycles with $\varepsilon_{m,1} = \varepsilon_{m,2} = 100\%$ according to the procedure described in Section 2.3. In Fig. 6 the complete temporal development of the extension $\varepsilon_x(t)$ of <PLAw0>, <PLAw1> and <PLAw2> models (averaged each over three packing models) in a time period of 20 ns including 1st and 2nd test cycle is displayed. Here it becomes obvious that in contrast to the first shape-memory cycle, where a faster recovery of PLAw2 was observed in combination with higher R_r (1) values in comparison to PLAw0 and PLAw1 (as discussed before), all samples exhibited an almost identical recovery behavior reaching $\varepsilon_{p,2}$ values in between 40% and 50%. The shape fixity remained constant in both cycles for all samples at around 90%. Almost identical values in the range of 61%-64% for R_r (1) and R_r (2) were obtained for PLAw0 and PLAw1, whereas for PLAw2 system R_r was found to decrease from 76% to 52% in two successive cycles (see Table 1). We anticipate that these findings can be explained by the fact that the initial structural differences between the unstretched samples (e.g. free volume distribution) are not longer present after completion of the first test cycle for dry and water swollen samples. Here the first cycle acts as a thermomechanical training procedure resulting in a similar pre-orientation status of the PLLA chains independent from the amount of incorporated water, which is determining the shape-memory behavior in the following test cycle.

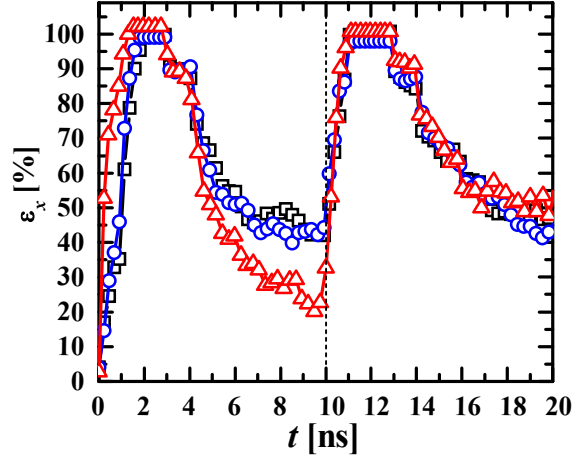


Fig. 6. Combined presentation of 1st (up to $t \leq 10$ ns) and 2nd ($t > 10$ ns) shape-memory cycle of PLAw0, PLAw1 and PLAw2 samples. <PLAw0>: open black squares, <PLAw1>: open blue circles, <PLAw2>: open red triangles.

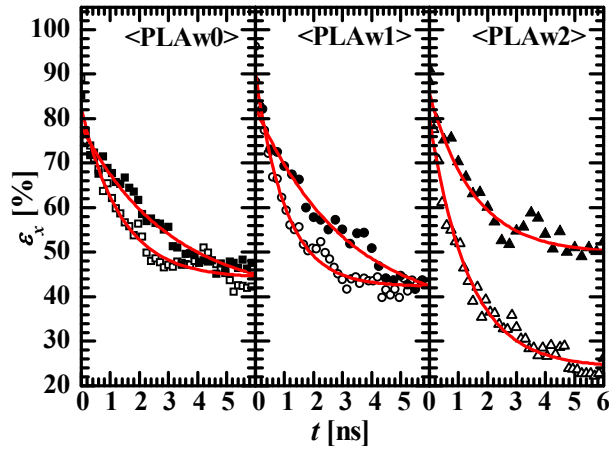


Fig. 7. Temporal development of the averaged extensions during recovery processes obtained in the 1st (open symbols) and 2nd cycle (solid symbols) for PLAw0 (squares), PLAw1 (circles) and PLAw2 (triangles) stretched up to $\varepsilon_m = 100\%$.

We attribute the observed slower recovery in the second test cycle (Fig. 7 and Table 2) to the higher degree of orientation of the PLLA chains reached after the first (training) cycle was completed and which should result in a decrease in entropy of the models and in this way lower recovery kinetics.

4. Conclusion

Recently we have introduced an atomistic modeling approach, which allows to describe two subsequent thermomechanical test cycles. In the present work we studied the influence of incorporating water molecules as well as the application of various deformations ε_m during

programming in two subsequent test cycles on the shape-memory behavior of amorphous PLLA switching domains.

It could be shown that the addition of 1 wt% and 2 wt% of water content caused a swelling effect D of the PLLA model samples of about 2% and 4% respectively. Moreover, the accessible fractional free volume was found to increase with increasing amount of water, while the simulated glass transition temperature T_g decreased from $T_g = 377$ K for the dry PLLA model to 322 K for PLAw2 containing 2 wt% of water.

Dry PLLA models and models with 1 wt% water content exhibited almost similar shape-memory properties in both subsequent test cycles with high shape fixity values of $R_f = 89\%$ - 92% and fair shape recovery ratios in the range of $R_r = 61\%$ - 64% when a ϵ_m of 100% was applied. Moreover, the increasing R_f and decreasing R_r values were achieved when ϵ_m was raised from 50% to 150% for such models. Analysis of the kinetic processes revealed that the relaxation kinetics during unloading was not affected by variation of ϵ_m while the recovery kinetics was accelerated with increasing ϵ_m . Furthermore, the recovery kinetics in the second cycle was found to be significantly decelerated compared to the previous first test cycle conducted under identical conditions.

The incorporation of 2 wt% water into the PLLA models was found to result in a different shape-memory behavior, where similar R_f and higher R_r values as well as a slower unloading relaxation process were obtained, which were not influenced by the application of different deformations. In contrast, the shape-memory properties observed in the second test cycle after completion of the first (training) cycle were almost similar to that of dry PLLA models.

In this work we could demonstrate that the initial structural properties of the simulated PLLA models before application of a shape-memory test are essential for the achievable shape-memory behavior. Whereby these initial structural properties such as the free volume elements distribution of PLLA can be influenced by the addition of water molecules or degree of orientation of the polymer chains by application of a training cycle.

We anticipate that the presented findings might motivate further atomistic modeling based research for prediction of the shape-memory properties of polymers, which could be extended in a next step to investigate e.g. the influence of arising degradation products on the shape-memory effect of degradable polymers or a shape-memory effect initiated by swelling in water.

Acknowledgements

E.G. is grateful to Berlin-Brandenburg School for Regenerative Therapies for a fellowship (DFG-GRS 203).

Appendix A: Supplementary data

Supplementary data related to this article can be found at <http://dx.doi.org/10.1016/j.polymer.2013.05.064>.

References

1. Lendlein A, Behl M, Hiebl B, and Wischke C. *Expert Review of Medical Devices* 2010;7(3):357-379.
2. Wischke C and Lendlein A. *Pharmaceutical Research* 2010;27(4):527-529.
3. Wischke C, Neffe AT, and Lendlein A. *Advances in Polymer Science* 2010;226:177-205.
4. Hu J, Zhu Y, Huang H, and Lu J. *Progress in Polymer Science* 2012;37(12):1720-1763.
5. Hu J, Meng H, Li G, and Ibekwe SI. *Smart Materials and Structures* 2012;21(5):053001.
6. Xie T. *Polymer* 2011;52(22):4985-5000.
7. Behl M, Ridder U, Feng Y, Kelch S, and Lendlein A. *Soft Matter* 2009;5(3):676-684.
8. Sauter T, Heuchel M, Kratz K, and Lendlein A. *Polymer Reviews* 2013;53:6-40.
9. Choi J, Ortega AM, Xiao R, Yakacki CM, and Nguyen TD. *Polymer* 2012;53(12):2453-2464.
10. Yang B, Min Huang W, Li C, and Hoe Chor J. *European Polymer Journal* 2005;41(5):1123-1128.
11. Sun L and Huang WM. *Materials & Design* 2010;31(5):2684-2689.
12. Chen S, Hu J, Yuen C-W, and Chan L. *Polymer* 2009;50(19):4424-4428.
13. Huang WM, Yang B, An L, Li C, and Chan YS. *Applied Physics Letters* 2005;86(11):114105.
14. Pierce BF, Bellin K, Behl M, and Lendlein A. *International Journal of Artificial Organs* 2011;34(2):172-179.
15. Yu YJ, Hearon K, Wilson TS, and Maitland DJ. *Smart Materials & Structures* 2011;20(8):085010.
16. Yang B, Huang WM, Li C, and Li L. *Polymer* 2006;47(4):1348-1356.
17. Kratz K, Narendra Kumar U, Nöchel U, and Lendlein A. *Materials Research Society Symposia Proceedings* 2012;1403:73-78.
18. Wagermaier W, Kratz K, Heuchel M, and Lendlein A. *Advances in Polymer Science* 2010;226:97-145.
19. Li G and Nettles D. *Polymer* 2010;51(3):755-762.
20. Kolesov IS, Kratz K, Lendlein A, and Radusch H-J. *Polymer* 2009;50(23):5490-5498.
21. Schmidt C, Chowdhury AMS, Neuking K, and Eggeler G. *Journal of Thermoplastic Composite Materials* 2011;24(6):853-860.
22. Schmidt C, Neuking K, and Eggeler G. *Mater. Res. Soc. Symp. Proc.* 2009;1190:43-48
23. Zhang Q and Yang QS. *Journal of Applied Polymer Science* 2012;123(3):1502-1508.

24. Qi HJ and Dunn ML. Thermomechanical Behavior and Modeling Approaches. In: Leng J and Du S, editors. Shape-Memory Polymers and Multifunctional Composites: Taylor & Francis, 2009. pp. 65-90.
25. Tobushi H, Okumura K, Hayashi S, and Ito N. Mechanics of Materials 2001;33(10):545-554.
26. Liu YP, Gall K, Dunn ML, Greenberg AR, and Diani J. International Journal of Plasticity 2006;22(2):279-313.
27. Nguyen TD, Yakacki CM, Brahmabhatt PD, and Chambers ML. Advanced Materials 2010;22(31):3411-3423.
28. Kolesov IS, Dolynchuk O, and Radusch HJ. Advances in Science and Technology 2012;77:319-324.
29. Diani J and Gall K. Smart Materials & Structures 2007;16(5):1575-1583.
30. Zhang CL, Hu JL, Ji FL, Fan Y, and Liu Y. Journal of Molecular Modeling 2012;18(4):1263-1271.
31. Bonner M, de Oca HM, Brown M, and Ward IM. Polymer 2010;51(6):1432-1436.
32. Heuchel M, Cui J, Kratz K, Kosmella H, and Lendlein A. Polymer 2010;51(26):6212-6218.
33. Wong YS, Stachurski ZH, and Venkatraman SS. Polymer 2012;52(3):874-880.
34. Ghobadi E, Heuchel M, Kratz K, and Lendlein A. Macromolecular Chemistry and Physics 2013; 214(11):1273-83.
35. Ghobadi E, Heuchel M, Kratz K, and Lendlein A. Journal of Applied Biomaterials & Functional Materials 2012;10(3):259-264.
36. Du A, Koo D, Ziegler M, and Cairncross RA. Journal of Polymer Science Part B- Polymer Physics 2011;49(12):873-881.
37. Yoon JS, Jung HW, Kim MN, and Park ES. Journal of Applied Polymer Science 2000;77(8):1716-1722.
38. Sun H. Journal of Physical Chemistry B 1998;102(38):7338-7364.
39. Theodorou DN and Suter UW. Macromolecules 1985;18(7):1467-1478.
40. Hofmann D, Fritz L, Ulbrich J, Schepers C, and Bohning M. Macromolecular Theory and Simulations 2000;9(6):293-327.
41. Berendsen HJC, Postma JPM, Vangunsteren WF, Dinola A, and Haak JR. Journal of Chemical Physics 1984;81(8):3684-3690.
42. Andersen HC. Journal of Chemical Physics 1980;72(4):2384-2393.
43. Heuchel M, Boehning M, Holck O, Siegert MR, and Hofmann D. Journal of Polymer Science Part B-Polymer Physics 2006;44(13):1874-1897.
44. Graziano G and Lee B. Biophysical Chemistry 2002;101:173-185.
45. Leach AR. Molecular Modelling: Principles and Applications Second ed. Dorchester: Prentice Hall, Pearson Education 2001.
46. Gestoso P and Brisson J. Journal of Polymer Science Part B-Polymer Physics 2002;40(15):1601-1625.
47. Zoller PW, Walsh D.J. Standard Pressure-Volume-Temperature Data for Polymers. Lancaster, PA: Technomic, 1995.
48. Entrialgo-Castano M, Lendlein A, and Hofmann D. Advanced Engineering Materials 2006;8(5):434-439.
49. Ghobadi E, Heuchel M, Kratz K, and Lendlein A. Journal of Applied Biomaterials & Functional Materials 2012;10(3):293-301.
50. Chow TS. Macromolecules 1980;13(2):362-364.
51. Zhang J, Yan JZ, Uitenham L, and Lou JZ. Study of the Molecular Weight Dependence of Glass Transition Temperature for Amorphous Poly(L-Lactide) by Molecular Dynamics Simulation. New York: Springer, 2009.
52. Jamshidi K, Hyon SH, and Ikada Y. Polymer 1988;29(12):2229-2234.

53. Hancock BC and Zografi G. *Pharmaceutical Research* 1994;11(4):471-477.
54. Bras AR, Viciosa MT, Dionisio M, and Mano JF. *Journal of Thermal Analysis and Calorimetry* 2007;88(2):425-429.